PRACE NAUKOWE Wyższej Szkoły Pedagogicznej w Częstochowie
Seria: FIZYKA z. IV, 2001

I.V. KITYK, M. MAKOWSKA-JANUSIK, J. BERDOWSKI
***M.D. FONTANA, M. AILLERIE AND F. ABDI**
Institute of Physics WSP, PL-42201, Al. Armii Krajowej 13/15, Częstochowa, Poland
**Laboratoire Materiaux Optiques a Proprietes Specifiques, CLOES, University of Metz and Supelec, 57070 Metz, Cedex, France*

Influence of Non-stoichiometric Defects on Optical Properties in $LiNbO_3$

1. Introduction

Is was recently reported that the optical properties of pure $LiNb0_3$ (LN) crystals are sensitive to the presence of the intrinsic defects related to the non-stoechiometry of the crystals [1]. Additionally, the electro-optic [2] and non linear optical properties [1] were shown to be strongly dependent on the concentration of these intrinsic defects.

This can lead to some problems in the use LN crystals in technological applications. It is therefore of prior importance to control the real composition of the crystal, or its deviation from the stoichiometric composition.

The parameter X_c, defined as the ratio between the Li concentration and the total amount of cations is introduced to characterise the deviation from the stoichiometry. Thus $X_c = 48.6\%$ is the composition in the congruent crystal whereas $X_c = 50\%$ corresponds to the stoichiometric composition. Various methods have been established to determine the crystal composition X_c [2]. Among them, the calibration of crystals from measurements of the refractive index [3], the absorption band edge [4] or the Raman phonon linewidth [5] provide accurate and consistent results.

Up to now, no theoretical investigations on calculations are available that are concerned with the microscopic origin and the physical mechanisms explaining the large dependencies of linear and non linear optical properties on the composition X_c.

All the previous considerations of the non-linear optical susceptibilities in congruent LN were based on a phenomenological bond length approach [6]. However it is obvious that in the case of LN single crystals neglecting by the long order crystalline band energy structure contributions to the band energy could lead to an essential error in determining how much local rearrangements contribute to the non-linear optical susceptibility. Recently [2] it was shown that stoichiometric pure LN crystals long-range crystal interactions contribute at least 16% for pure electronic and about 9% for the phonon part. An over-simplified cluster approach to evaluate the non-linear optical susceptibility was usually used and the long range contributions were calculated using re-normalization of only a macroscopic dielectric susceptibility.

Such an approach could be partially suitable for an ideal (perfect) crystalline but is absolutely insufficient for doped crystalline systems. To resolve the problems mentioned above we will consider the band energy for the perfect (pure stoichiometric) crystal and then take into account existing defect states. The latter can be considered as a modulation of the ideal crystalline structure by the long-range defect fields. In our considerations we suppose that Nb atoms substitute Li on the so-called Nb antisites and as a consequence we have local structural rearrangement with creation of the near-the-Li oxygen vacancies and Nb_{Li} antisites. Based on the band energy structure calculations, we evaluate spectral dependencies of the imaginary part of the dielectric susceptibility for various values of the parameter X_c and determine particular contributions of the different cluster groups to the optical spectra. The similar approach has been successfully applied by us to the disordered materials: glasses [7], guest-host polymers [8] complex and doped crystals [9]. The investigated LN crystals can be considered as a slightly disordered crystals. As a consequence, the mentioned approach may be used. We have revealed that for an explanation of optical spectra and especially nonlinear optical properties a better agreement has been achieved using norm-conserving pseudopotential (NCPP) method because the optical effects are determined first of all by the external valence electrons and unoccupied excited states. Unfortunately self-consistent eigenenergy convergence within a framework of the one-electron band energy calculations is not sufficiently enough for performing of the molecular dynamics geometry optimisation. Therefore additional molecular dynamics procedure is necessary. As the external electrostatic field we used one-electron band energy solid state calculations [10]. In the case of the second-order nonlinear optical effects (particularly, of the optical second harmonic generation), contrary to the usual optical effects, the non-centrosymmetry in the charge density distribution plays a key role [11]. Therefore appropriate connection of the solid state approach with the local structure optimisation will be applied. Moreover, in the case of the linear electrooptics substantial contribution gives phonon subsystems.

Therefore main principles of our approach are the following:

— band energy structure calculations of the LN using *ab initio* norm conserving pseudopotential method for the pure and non-steichiometric specimens;

— determination of the optical constants depending on the degree of non-steichiometry;

— calculations of the [Nb-O_6] cluster charge density distribution without and with taken into account of the molecular dynamics simulations and optimisation of the cluster geometry with taking into account a redistribution of the electrostatic potential space distribution within the clusters;

— simulation of electrooptics coefficients behaviour depending on the non-steichiometry with taken into account of the electron and phonon subsystems;

Band energy structure for the LN crystals with the different X_C is presented in the Sec. 2. Molecular dynamics procedure and the geometry optimisation is reported in the Sec. 3. Structural rearrangements of particular clusters is presented depending on the non-stoichiometry. Sec. 4 presents the phonon contributions to the electrooptic coefficient r_{22} calculated for the crystals with various steichiometry. Particular contributions of the UV-electronic states modified by effective electron-phonon interactions are presented in the Sec. 5. A discussion concerning agreements and discrepancies between the proposed approach and experimental data is carried out.

2. Electronic structure of ln crystals with intrinsic defects

Up to now there is only one work devoted to *ab initio* band energy calculations of the LN single crystals that is in a satisfied agreement with the experimental X-ray photoelectron spectra. As a more efficient method of the band energy structure calculations for the such kinds of the systems seems to be the NCPP calculation method [12]. This concerns to the optical data. This method has been successfully applied for simulation of the optical spectra in the different crystalline as well non-crystalline systems [13] with presence of intrinsic as well extrinsic defects.

In this paper, we perform a detailed calculation of the band electronic structure and of the appropriate optical properties of the LN crystals using the first-principles NCPP method in the local approximation of density-functional theory. This method has been approved also during the calculations of the nonlinear optical properties of the complex systems [14], metallic glass sys-

tems [15], polymer-like systems [16] etc. The LN crystals with different non-stoichiometry can be considered as slightly disordered systems. Therefore an applying of the NCPP method to the mentioned systems seems to be reasonable.

The total energy functional was expressed within a framework of the local density functional approach and of a Hartree-Fock minimisation procedure and was carried out towards the charge density $\rho(r)$:

$$E_{tot}[\rho(r)] = T[\rho(r)] + V_{n\text{-}e}[\rho(r)] + V_{e\text{-}e}[\rho(r)] + V_{e\text{-}c}[\rho(r)], \quad (1)$$

$$\text{where } \rho(r) = \Sigma_{\beta,l}|\Psi(l,\mathbf{r},\beta)|^2. \quad (2)$$

Kinetic energy functional $T[\rho(r)]$ is calculated in the Thomas-Fermi free electron approach;

$V_{n\text{-}e}[\rho(r)]$ corresponds to nuclear-electron Coulomb-like interaction that in present case is chosen in the form described by [13]. A non-linear extrapolation procedure was conducted to evaluate the corresponding NCPP in the form convenient for the analytical evaluations (gaussian-polynomial-like), particularly:

$$V_{n\text{-}e}^{(\beta,l)}(r) = \Sigma_i(A_i{}^{\beta} + r^2 A_{i+3}{}^{\beta}\exp(-\alpha_n{}^{(l,,\beta)}r^2), \quad (3)$$

where β determine a kind of atom; l is an appropriate angular momentum; value of n depends on the precision of fitting procedure for the corresponding non-linear interpolation procedure and is varied within the 1 and 5. During the nonlinear interpolations NCPP has been expressed in form of at least 18 gaussian-polynomial orbitals with decaying exponents in the range 0.001– – 835000. The basic wave-functions consisted of 1s – 5d orbitals of Nb, 1s – – 3p orbitals of Li, and 1s – 4s orbitals of O. We have included excited orbitals in order to enhance precision of the matrix dipole momentum values, especially for optical properties simulation. The proposed approach allows to achieve the eigenvalue convergence up to 0.0013 eV. $V_{e\text{-}e}[\rho(r)]$ and $V_{e\text{-}c}[\rho(r)]$ are screening potentials corresponding to electron-electron and exchange-correlation interactions, respectively. Coefficients a and α are evaluated fitted coefficients determined by the non-linear extrapolating procedure.

The proposed form of the NCPP allows to obtain the corresponding matrix elements in an analytical form. All the procedure consists in a resolving of the following secular equation:

$$\|[h^2(k + G_{n,n'})^2/2m - E(k)]\delta_{n,n'} + \Sigma_\alpha V_\alpha(\mathbf{G_n}' - \mathbf{G_n})S_\alpha(\mathbf{G_n}' - \mathbf{G_n})\| = 0 \quad (4)$$

where $E(\mathbf{k})$ is the searched eigenenergy for a given $\mathbf{k}$ point of the BZ; $\mathbf{G_n}'$ and $\mathbf{G_n}$ are interacting basis plane waves. For the stoichiometry specimens we have taken into account at least 3680 plane waves and additional 1244 plane waves were taken in the Lowdin perturbation approximation. As a criterion of the convergence was chosen the stability of the eigenenergy within the 0.0015 eV. After undergoing to the non-stoichiometric cases we have taken into account at least 4286 and 1346 plane waves respectively. We have found that increase of the convergence limit from 0.02 eV up to 0.002 eV causes maximal shift of the particular energy bands less than 0.04 eV that corresponds to the changes of the matrix dipole moments less than 8.2%.

Resolving of the mentioned secular equations was carried out using the QL-modified Jacobi method. The structural factor for the β kind of atom was evaluated in the form:

$$S_\beta^{(\alpha)}(\mathbf{G_n}' - \mathbf{G_n}) = g^{(\alpha)}/N\Omega\Sigma\beta\exp[-i(\mathbf{G_n}' - \mathbf{G_n})\tau\beta] \quad (5)$$

Here $g^{(\alpha)}$ corresponds to the particular contributions of the α-th ions and is given by the stoichiometry X_C. Varying the weighting coefficients $g^{(\alpha)}$ we obtained the band energy structures for the given non-stoichiometry. The Fourier transformations of the pseudopotential for the α-th kinds of ions take a form:

$$V_\alpha^{(\alpha)}(\mathbf{G_n}' - \mathbf{G_n}) = 1/\Omega\int V^{(\alpha)}(\mathbf{r})\exp[-i(\mathbf{G_n}' - \mathbf{G_n})\mathbf{r}]\, d^3\mathbf{r} \quad (6)$$

Electron screening effects were calculated using parametrised Perdew-Zunger [17] and Ceperley-Alder expressions [18].

A special method of Chadhi-Cohen [19] was used for calculation of the space electron charge density distribution. The latter was used to construct the charge density functional of electrons. The diagonalization procedure was performed in the 32 special points of the Brillouin zone (BZ) and afterwards an extrapolation was done using a perturbation **kp** method.

Acceleration of the iteration convergence was done by mixing the (m-1)-th iteration with the 70% of the output ρ before their substitution into the next equation. A criterion of the self-consistence was satisfied after ensuring the condition:

$$|\rho_{out,m} - \rho_{inp,m}| < \varepsilon \qquad (7)$$

after the m-th iteration step. We assumed an accuracy less than $\varepsilon = 8.5\%$ between the input and output iterations as a main criterion of the self-consistence. The energy eigenvalues were stable within a range of 0.002 eV. The numerical evaluations of the charge density functional terms were carried out using a numerical tetrahedral method with an increment about 0.002 Hartree.

We started the calculations for the perfect stoichiometric crystals with the factor $g^{(\alpha)}$ equal to 1. Afterwards the factors $g^{(\alpha)}$ have been varied appropriately to the given X_C. All the calculations have been performed for the 412 points of the BZ. The general form of the band energy dispersion was in agreement with the obtained in the Ref. [20].

Comparing the calculated bands with the experimental data on the X-ray photoelectron spectroscopy [21] we revealed an agreement up to 0.17 eV. The value of calculated energy gap was less than 3.69 eV comparing with the 3.80 eV obtained from the absorption edge. Refractive index was equal about 2.1578 that is very close to the experimentally measured 2.1397 [2]. All these data show that the adopted approach is sufficient for explaining of the main optical parameters. We have found that maximal deviation from the perfect band structure is observed for the $X_C = 48.4\%$. On the ground of the performed band energy calculations we performed evaluations of the imaginary part of the dielectric susceptibility using the equation:

$$\varepsilon_2(E) = 2\pi Ne^2/h^3 \sum_{v.b.k} \int |< \Psi_{v.b.}(\mathbf{k},\mathbf{r})| \Psi_{c.b.}(\mathbf{k},\mathbf{r})|> d^3\mathbf{r}\, \delta(E_{v.b}(\mathbf{k}) - E_{c.b}(\mathbf{k}) - E), \quad (8)$$

where $\Psi_{v.b.}(\mathbf{k},\mathbf{r})$ and $\Psi_{c.b.}(\mathbf{k},\mathbf{r})$ correspond to the valence and conduction band pseudowavefunctions, respectively. All the summation is performed over the whole Brillouin zone. In the Fig. 2 are reported the spectral dependence of the imaginary fart of the dielectric susceptibility $\varepsilon_2(E)$ for the crystals with various compositions, as calculated by the above methods. In the Fig. 1 are presented experimentally measured (points) and solid full lines (the theoretically calculated) of imaginary part of dielectric susceptibilities.

The changes in the energies are more clearly for the bands (indicated by B and C) originating prevailingly from the 2p O orbitals. This one once more confirm that the main changes of the band electron structure are originated from the delocalised oxygen states. The 4d Nb states (by the number A in the Fig. 1) forming the conducting band states are more less dependent on the X_C. Core-like 2sO band are independent on the X_C.

First of all we should point out an appeared anisotropy of energy dispersion with decreasing X_C. This is caused by anisotropy in the localisation of

the corresponding band carriers. The presented data unambiguously indicate that the non-stoichiometry essentially influence on the density of states and on the carrier effective mass determining the band electron localisation. The

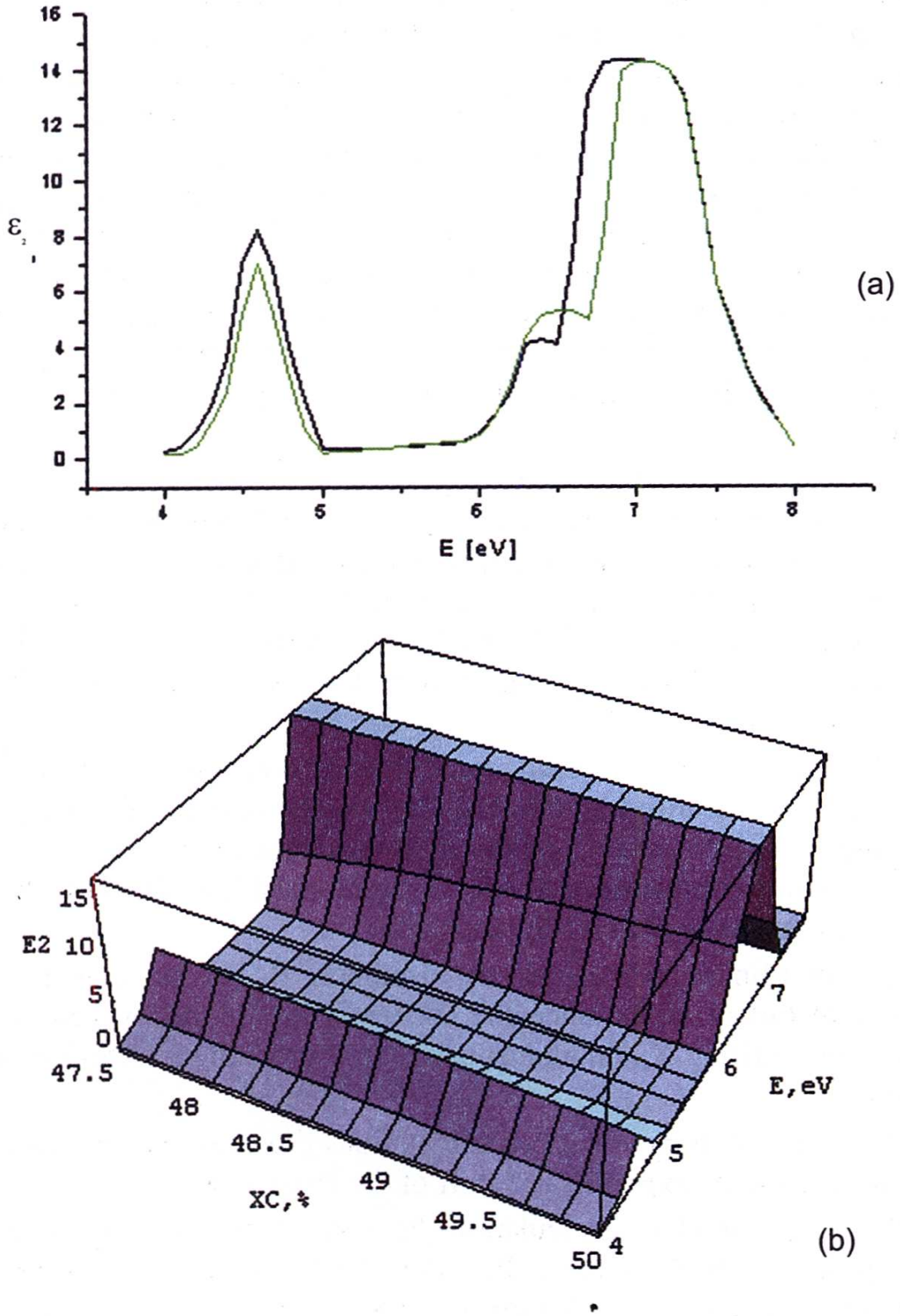

Fig. 1. Imaginary part of the dielectric susceptibility ε_2 versus the energy E, as calculated in crystals with various compositions X_C. 1 a: Two-dimensional representation – green line – experimental; black – computed: X_C = 50 % – – continuous line: X_C = 48.5%; 1 b: Three-dimensional representation

increase of the carrier localisation was revealed for the $X_C = 48.4\%$. For the $X_C = 49.5\%$ this localisation drastically decreases. And for the $X_c = 49.5\ \%$ the localisation is maximally similar to the perfect LN crystals. More prominent this dependence is presented in the three-dimensional Fig. 1b. Such complicated dependencies of the band energy localisation reflects a competition between the long-range crystalline ordering in the perfect crystals and local disorder due to the oxygen defect presence. The maximal deviations comparing with the perfect crystals in the band energy dispersion are up to the 0.22 eV. But the performed minimisation procedure within a framework of one-electron approach is not satisfactory enough for the total energy minimisation within the particular structural clusters. Similarly as in the case of the disordered materials [7] in the non-steichiometry LN crystals we should do additional molecular dynamics simulations within the particular clusters in order to explain the observed changes of the non-cetrosymmetry and of the corresponding electrooptics coefficients described by the third order polar tensors.

Fig. 2 a exhibits three maxima successively labeled A, B and C around 4.8, 6.32 and 6.88 eV, respectively. They correspond to the inter-band optical transition oscillators originating from the two structural clusters. The oscillator A is originated from the intracluster 4d Nb-2p O relatively localised states whereas the other oscillators B and C come from the 2p 0 – 2s Li states. As shown in the Fig. 1–b, the intensities of the peak A, B and C change with varying the composition X_C.

The intensity of C is nearly constant and therefore is related to the long-range highly delocalised 2p 0 – 2s Li hybridised orbitals. The peaks A and B show opposite dependencies on the X_c. The exponentially-like decrease of the first oscillator with raising xc reflects the diminishing content of the Nb ions on the Li site (the so called Nb_{Li} antisites).

The non-linear increase of the oscillator B can be related to oxygen-vacancy disturbed states since the concentration of the oxygen-vacancy decreases with raising X_c simultaneously with increasing Li sites occupation by Li ions.

It can be mentioned that our calculations (decrease of the peak A) are in agreement with the experimental shift of the energy gap with X_c.

The performed by us calculations have shown that increase of the convergence limit from 0.02 eV up to the 0.00042 eV changes the appropriate dipole momentums less than 9%. Therefore in order to evaluate the observed changes of the optical constants (not the values) in the electrooptics behaviour versus the steichiometry it is sufficient to carry out the simulations with the convergence limit within the 0.02 – 0.002 eV.

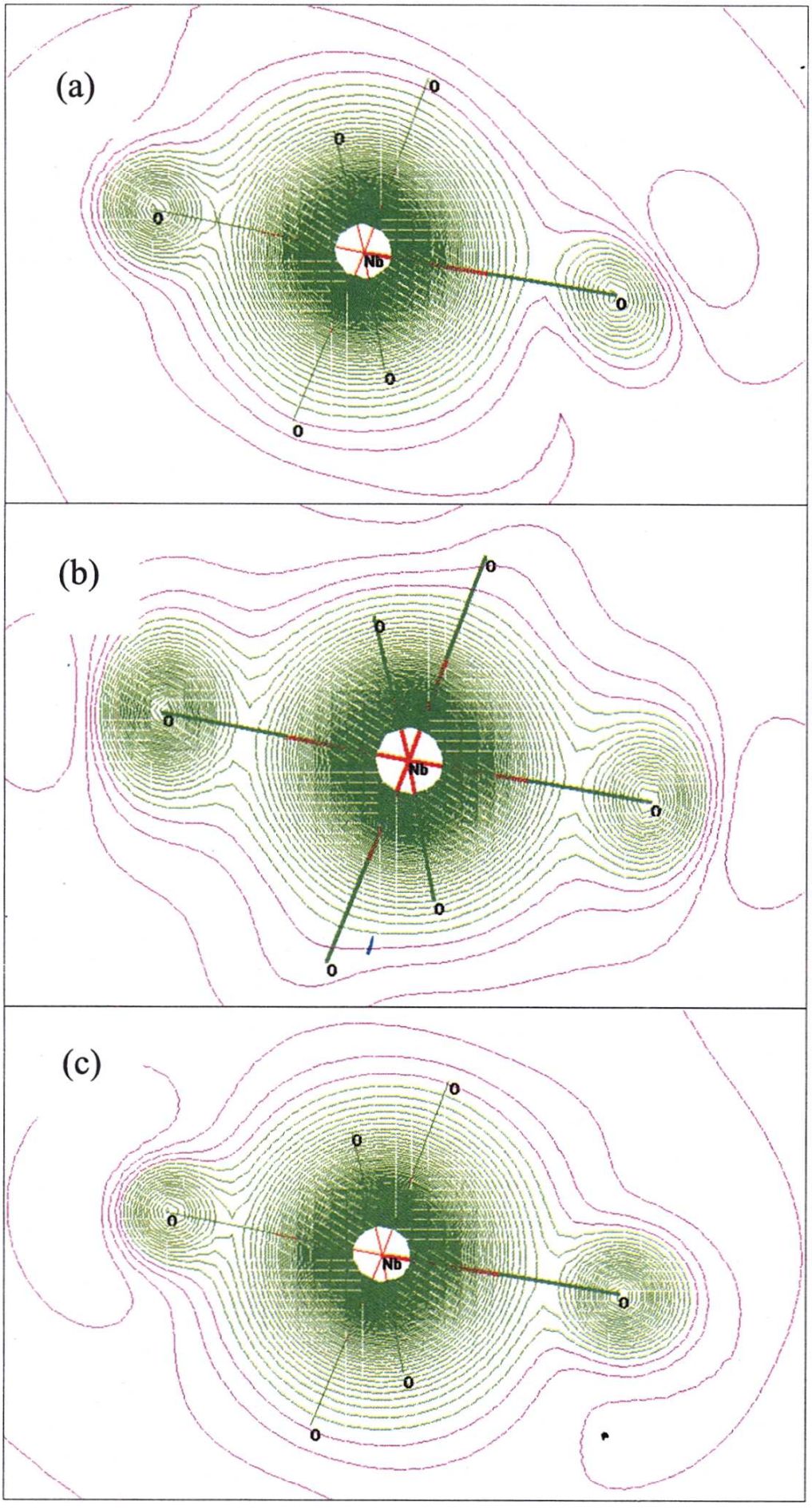

Fig. 2. Electrostatic potential distribution around [Nb-O_6] clusters

The presented above results indicate that, even without the molecular dynamics near-the-defect structural rearrangement can explain main linear optical effects (absorption, refractive index etc) as well the band energy wide (X-ray-photoelectron spectroscopy). However, this approach is not enough for explanations of the nonlinear optical properties, particularly of the electrooptical effects. This problem will be considered in the next section. We have checked also that the contributions of the more higher energy oscillators with the energies higher than 7.5 eV create only an effective background that is non-sensitive to the non-stoichiometry.

3. Molecular dynamics simulations

In the Sec.2 we have proved that the band energy calculations show opposite behaviours versus X_c for the main optical oscillators, even if the local structural rearrangement due to the presence of the intrinsic defects may be neglected. In the present section we will show how the band energy contributions disturb the local clusters $Nb0_6$ or $Li0_6$. For this reason, we use *ab initio* molecular dynamics geometry optimisation.

As a starting point we have used hybrid Becke's method [22] using the elecrostatic potential parameters obtained from the *ab initio* band energy structure calculations. The main advantages of the mentioned method consists in a very fast convergence of the eigenvalues with respect to the size of the basis sets. Geometry optimisation for each crystal composition was done using the gradient-corrected potential functional in the electrostatic potentials with the step of 0.05%, and the harmonic frequencies for subsequent calculations were determined by an analytical differentiation of the Hessian matrices.

The nondynamic correllations were taken into account within the molecular cluster self-consistent functional approach included in the GAMES program [22]. Geometry optimisations were performed using the gradient conditions of the GAMES program, and the dynamics boundary conditions have been applied. Afterwards we have calculated the matrix dipole moments. The equilibrium atom positions were obtained from a condition for the minimum of the total energy U_{tot}.

We have found that the picture around the clusters $Nb0_6$ is strongly dependent on the crystal composition, whereas the electrostatic potential around the $Li0_6$ cluster was nearly insensitive to a change of X_C. Therefore only the [Nb-O_6] clusters will be considered. Moreover it is well known from the more simpler approaches that these clusters play a key role in the observed effects.

From the Fig. 2 one can see a redistribution of effective electrostatic potentials depending on the non-stechiometry X_C obtained after and before the performed molecular dynamics geometry optimisation. For convenience one

can see a shift of the effective center position of the electrostatic potentials from equilibrium positions. One can see that for the $X_C = 48.7\%$ the distribution of the electrostatic potential in the XY-crystallographic plane is more centrosymmetric than comparing for the two other cases. For more clarification in the Table 1 are presented parameters of the cation-anion distances within the [Nb-O_6] cluster.

The presented data unambiguously show that the performed molecular dynamics geometry optimisations cause additional structural stabilisation (lowering of the total energy U_{tot}). The more interesting is the fact that the distances between the Nb-O(1) andf Nb-O(2) correlate well with the appeared non-centrosymmetry. Comparing the Fig. 2 and the Table data one can unambiguously say about essential role of the additional geometry optimisation for obtaining the more stable geometry structure (lower total energy) and appearance of the non-centrosymmetry in the electrostatic potential distribution.

Table 1. Main distances between the main ions within the [Nb-O_6] before and after the molecular dynamics geometry optimisation procedure

N	Before molecular dynamics simulation			After molecular dynamics simulation		
X_C,%	Nb-O(1), A	Nb-O(2), A	U_{tot}, eV	Nb-O(1), A	Nb-O(2), A	U_{tot}, eV
48.4	2.321(8)	2.304(7)	-22.12(0.02)	2.333 (0.012)	2.269(0.012)	-26.94(0.02)
48.7	2.313(3)	2.294(4)	-19.68(0.02)	2.304(0.012)	2.261(0.012)	-25.75(0.02)
49.5	2.302(1)	2.292(5)	-24.35(0.02)	2.319(0.012)	2.280(0.012)	-27.35(0.02)

The presented Table confirms the conclusion done for the disordered materials concerning a necessity of additional total energy optimisation within the particular structural clusters.

4. Phonon contributions to the electrooptic coefficients

It is well known that taking into account of the phonon states play an important role in the calculation of electro-optic coefficients. Therefore in this section we will attempt to evaluate the particular contributions of the phonon modes to the calculated electro-optic coefficient r_{22}. Such an approach was successfully developed for chalcogenide glasses and is here extended to the slightly disordered crystals (non-stoichiomtric LN).

The quantum chemistry calculations were performed self-consistently after separation of the electron and phonon contributions. The Schrodinger equation for a purely vibration motion was expressed within a harmonic approximation:

$$d^2\Psi_k/dQ_k^2 + [\ 8\pi^2 \mu_k h^{-2}\Omega_k - 4\pi^2\mu_k h^{-2}\Omega_k^2\ ]\ \Psi_k = 0, \qquad (9)$$

where Ψ_k is a wave function corresponding to k-th normal coordinate Q_k ; μ_k denotes a reduced mass of the nuclei taking part in the k-th vibration mode. It is obvious that solutions to the above equation are determined by a model which is responsible for the force constant calculations (so called Hessian matrices), i.e., the second derivatives of an electrostatic cluster potential with respect to given normal coordinates. All the phonon frequencies have been fitted to the experimental Raman data [5].

Besides the usual harmonic modes we have taken into account also electron-phonon interaction potential that was calculated in a nonlinear approximation[22]:

$$V_{e\text{-}ph}(\mathbf{r}_i) = e^2\sum_{ms} M_{ms}^{-1/2}\,[Z_{ms}(\mathbf{r}_s-\mathbf{u}_{ms})|\mathbf{r}_s-\mathbf{u}_{ms}|^{-3} - \sum_{m's'} Z_{m's'}(\mathbf{r}_{s'}-\mathbf{u}_{m's'})|\mathbf{r}_{s'}-\mathbf{u}_{m's'}|^{-3}], \qquad (10)$$

where M_{ms} and eZ_{ms} are the effective ionic mass and charge, the corresponding ions are labelled by m and s, respectively. The $\mathbf{u}_{ms,m's'}$ vector is a relative displacement of two ions from their equilibrium positions $\mathbf{r}_s$ and $\mathbf{r}_{s'}$. Probability of a one-phonon transition induced by the vibration of a frequency Ω_k is equal to:

$$W(\Omega_k) = 4(h/2\pi)^{-2}c^{-3}\,H^{-1}g^{-1}(\mathbf{r}_i)\,(\,E_{el} - \Omega_k\,)^2\,B(\Omega_k), \qquad (11)$$

where the η and the ξ are the lower and upper electron MO energy levels, respectively; H is a sum of the η and ξ levels widths, E_{el} is an energy of the inter-band transitions, Ω_k denotes a k-th phonon energy and $g(r_i)$ is a degeneration degree of the corresponding electron energy levels. The parameter $B(\Omega_k)$ is equal to [7]:

$$B(\Omega_k) = \sum_{\eta}^{g(\eta)}\sum_{\xi}^{g(\xi)} |\{\sum_{\varphi} \langle\eta,\eta_\Omega|V_{e\text{-}ph}(\mathbf{r}_i)|\varphi,\eta_{\Omega+1}\rangle\langle\varphi|\mathbf{d}|\xi\rangle\,(E_\xi-E_\eta+\Omega_k)^{-1} +$$

$$+ \sum_{\varphi} \langle\eta|\mathbf{d}|\varphi\rangle\langle\varphi,\eta_\Omega|V_{e\text{-}ph}(\mathbf{r}_i)|\xi,\eta_{\Omega-1}\rangle\,(E_\xi-E_\eta-\Omega_k)^{-1}\}|^2_\theta, \qquad (12)$$

where φ denotes a virtual intermediate band states, $\mathbf{d}$ is an electric dipole moment for a given optical transition. The summation is performed over all degenerated initial and final states. The notation θ denotes an averaging with respect to occupation numbers of the quasi-phonon states. We have checked that an increase of the oxygen content favours an occurrence of the hexagonal structural fragments that are typical for the pure quartz single crystals.

Our calculations have shown that dominant role in the corresponding electrooptics coefficients give the Li-O clusters because they give more higher frequency resonance and are more sensitive to the disturbed by the Nb antisites oxygen vacancies. But we consider also the [Nb-O_6] clusters and inter-the-cluster bridges in the first perturbation approach.

On the other hand, the phonons included in the electron-phonon interaction (Eq. 12) can lead to the following normal coordinates:

$$B(\Omega_k)= C_{\eta\xi}^{\gamma}(r_\lambda^{\Delta}) C_{\eta\xi}^{\gamma'}(r_{\lambda'}^{\Delta'}) \operatorname{Im} G_{\Delta\Delta'}^{\gamma\gamma'}(r_\lambda^{\Delta}, \Omega_k^2), \qquad (13)$$

where $G_{\Delta\Delta'}^{\gamma\gamma'}(r_\lambda^{\Delta})$ is a Green function (γ and γ' are numbers of coordination sphere) defined as:

$$G_{\Delta\Delta'}^{\gamma\gamma'}(r_\lambda^{\Delta}) = \sum_{\varphi} \{\langle\eta|V_{e\text{-}ph}(\mathbf{r}_i)|\varphi\rangle\langle\varphi|\mathbf{d}|\xi\rangle + \langle\eta|\mathbf{d}|\varphi\rangle\langle\varphi|V_{e\text{-}ph}(\mathbf{r}_i)|\xi\rangle \}(E_\xi - E_\eta)^{-1}. \qquad (14)$$

The resulting expression is given below:

$$G_{\Delta\Delta'}^{\gamma\gamma'}(r_\lambda^{\Delta}, \Omega_k^2) = \sum_{\Omega} K_{\Delta'}^{\gamma'}(r_\lambda^{\Delta}) K_{\Delta}^{\gamma}(r_\lambda^{\Delta}) (\Omega_k^2 - \Omega^2 - i\delta)^{-1}, \qquad (15)$$

where the coordinates $K_{\Delta}^{\gamma}(r_\lambda^{\Delta})$ are obtained for a given phonon mode from the electron states averaging. To include the local lattice deformations into the Green function, we have taken into account also the [Li-O] deformation localisation that allows to use the Dyson relations. The deformation potential and corresponding oxygen-vacancy charge defect disturbance determine the potential operator U and:

$$G_{\Delta\Delta'}^{\gamma\gamma'}(1) = G_{\Delta\Delta'}^{\gamma\gamma'}(0) + G_{\Delta\Delta'}^{\gamma\gamma'}(0)\, U\, G_{\Delta\Delta'}^{\gamma\gamma'}(1), \qquad (16)$$

where $G_{\Delta\Delta'}^{\gamma\gamma'}(0)$ and $G_{\Delta\Delta'}^{\gamma\gamma'}(1)$ are the Green functions for ideal and system with defects, respectively.

The relation between real and imaginary parts of the Green function were evaluated using Kramers-Kronig dispersion relations. The main phonon contributions come from modes with relatively high frequency originating from the [Li-O] intracluster. All the phonon modes were renormalised by electron-phonon nonlinearities described above.

The contribution of the phonons to the electrooptic coefficients was calculated using the general following expression:

$$X_{ijk}^{(\omega,\omega)} = \frac{1}{h^2}\frac{e^3 N}{2!}\hat{P}_{ijk}\sum_k\sum_{\alpha,\beta}\left[\frac{\langle 0|i|\alpha\rangle\langle\alpha|j|\beta\rangle\langle\beta|k|0\rangle}{(2\omega + \omega_\alpha^*)(\omega + \omega_\beta)} + \right.$$
$$\left. + \frac{\langle 0|j|\alpha\rangle\langle\alpha|i|\beta\rangle\langle\beta|k|0\rangle}{(\omega_\alpha - 2\omega)(\omega_\beta - \omega)} + \frac{\langle 0|j|\alpha\rangle\langle\alpha|k|\beta\rangle\langle\beta|i|0\rangle}{(\omega + \omega_\beta)(\omega_\alpha - \omega)}\right. \qquad (17)$$

where $\Omega_{\alpha,\beta}$ are eigen-frequency phonon modes; <A|i|B> are phonon mode dipole matrix elements disturbed by the electron-phonon interactions to calculate the particular EO coefficient r_{22},we put i = j = k = 2 in eq.21. We have performed all calculations for the Γ point of the BZ. All the taken into account phonon modes have been agreed with the experimentally by [5]. The presented calculations allow to detect the changes in the electrooptics coefficients up to the 0.2 pm/V. Because the main goal of the present work consists in the simulation of the changes of the r_{22} versus the non-steichiometry in the chosen model approach should be absolutely sufficient to determine the corresponding changes. The determination of the absolute values of the electrooptics coefficients is not a goal of the present work and will be a subject of a separate future work.

The calculations of the r_{22} were carried out separately for the harmonic phonon modes. Then we have superimposed phonon modes renormalised by the electron-phonon interactions. The contributions of each phonon mode to calculated electrooptic coefficient r_{22} were determined for crystals with various compositions X_c. The corresponding results are presented in Fig 3.

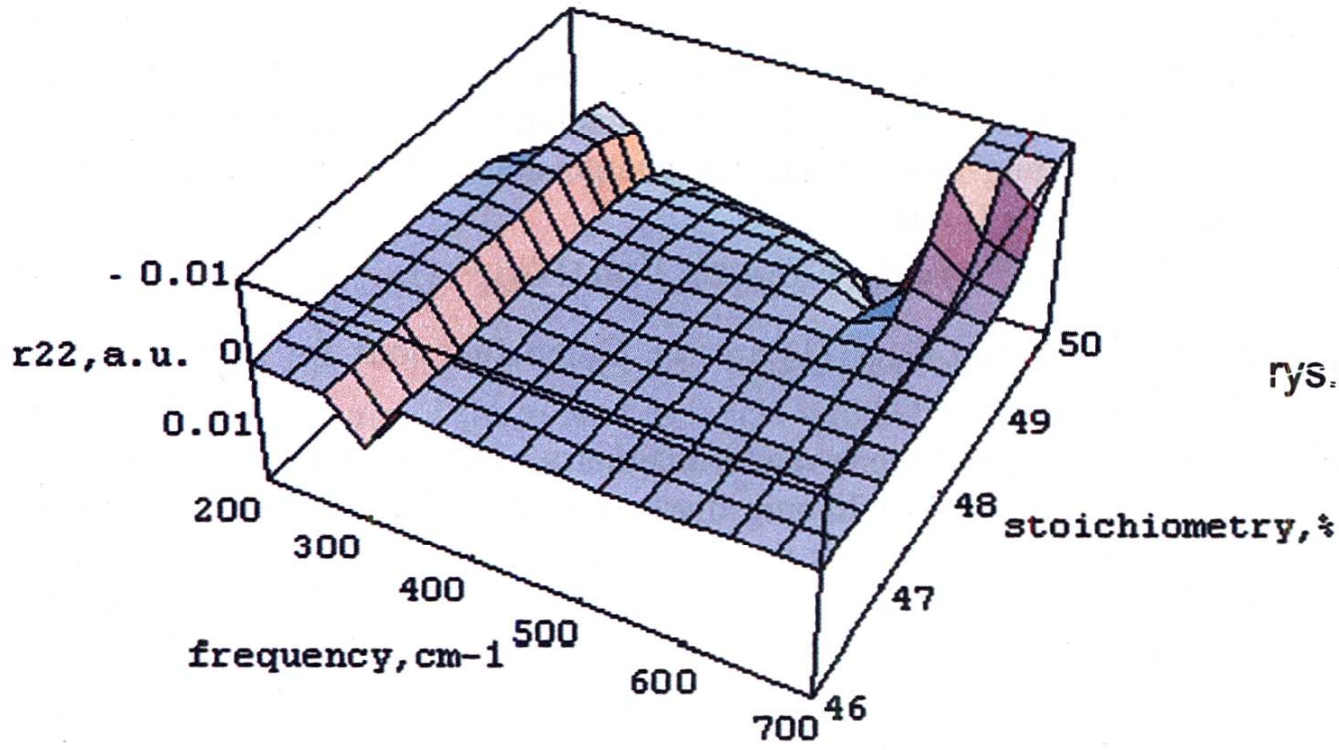

Fig. 3. Ionic (phonon) contribution to the electrooptic coefficient r_{22} as calculated from Eq. 17

First we can note the opposite signs of the particular phonon modes contributions to the electrooptic coefficient r_{22}. Most of the active phonon modes have positive sign contributions whereas the modes higher than 580 cm^{-1} give essentially opposite negative contributions which drastically increases with the parameter X_C. This proves that Li-O dipole plays key role in the large value of the EO coefficient r_{22} obtained in the stoichiometric crystal.

The physically origin of the opposite sign contributions can be attributed to different directions of the non-centrosymmetry within the Nb-O and Li-O shells.

5. Influence of the intrinsic non-stoichiometry on a dispersion of the electrooptic coefficients

The calculations of the electronic part of the electrooptic tensors have been carried out using the expression and the calculation techniques similar to the works [16]:

$$X_{ijk}^{(\omega,\omega)} = \frac{1}{h^2}\frac{e^3 N}{2!}\hat{P}_{ijk}\sum_k\sum_{\alpha,\beta}\left[\frac{<0|i|\alpha><\alpha|j|\beta><\beta|k|0>}{(2\omega+\omega_\alpha)(\omega+\omega_\beta)}+\right.$$
$$\left.+\frac{<0|j|\alpha><\alpha|i|\beta><\beta|k|0>}{(\omega_\alpha-2\omega)(\omega_\beta-\omega)}+\frac{<0|j|\alpha><\alpha|k|\beta><\beta|i|0>}{(\omega+\omega_\beta)(\omega_\alpha-\omega)}\right. \quad (18)$$

where the $<\alpha|y|\beta>$ are dipole matrix momentum between the α and β electronic band states; P is a permutation operator; N is the concentration of the valence electrons; the summation over the **k** means summation over the whole effective Brillouin zone.

Comparing the experimental data with the theoretically calculated (compare Fig. 4 a and 4 b) one can see a good agreement. It is necessary once more to underline that the developed approach is valuable for simulation of the changes of the electrooptics coefficients versus the non-steichiometry parameters. However in order to determine the absolute values of the electrooptics coefficients the precision of the dipole moments should be enhanced. Moreover, the experiment concerning determination of the absolute r_{22} electrooptics coefficient is not always sufficient for comparison with the theory. At the same time the changes give more important information for the technologist showing the main directions of the electrooptics r_{22} coefficients changes.

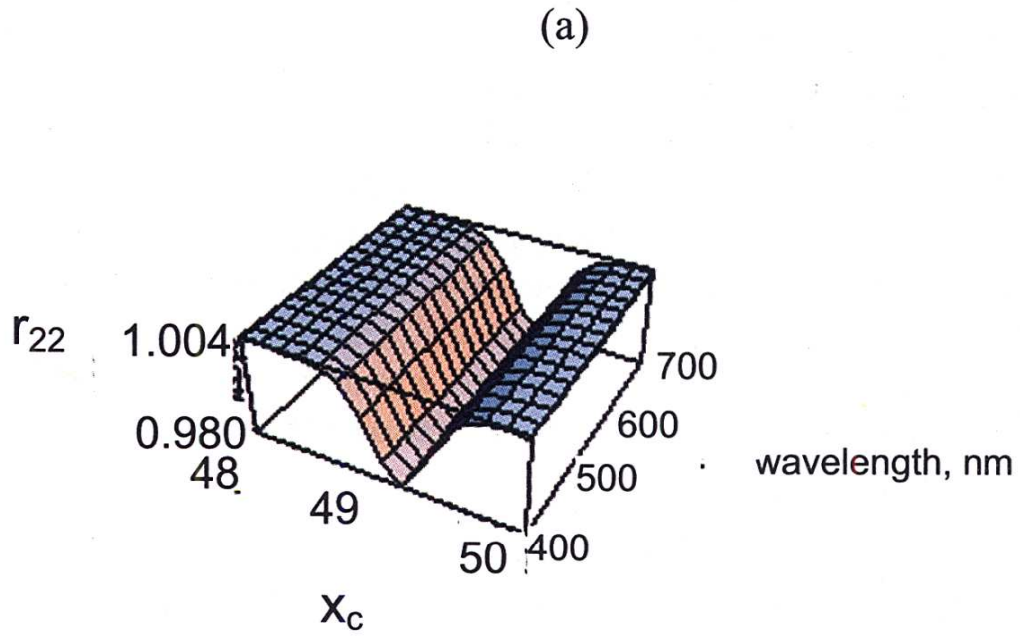

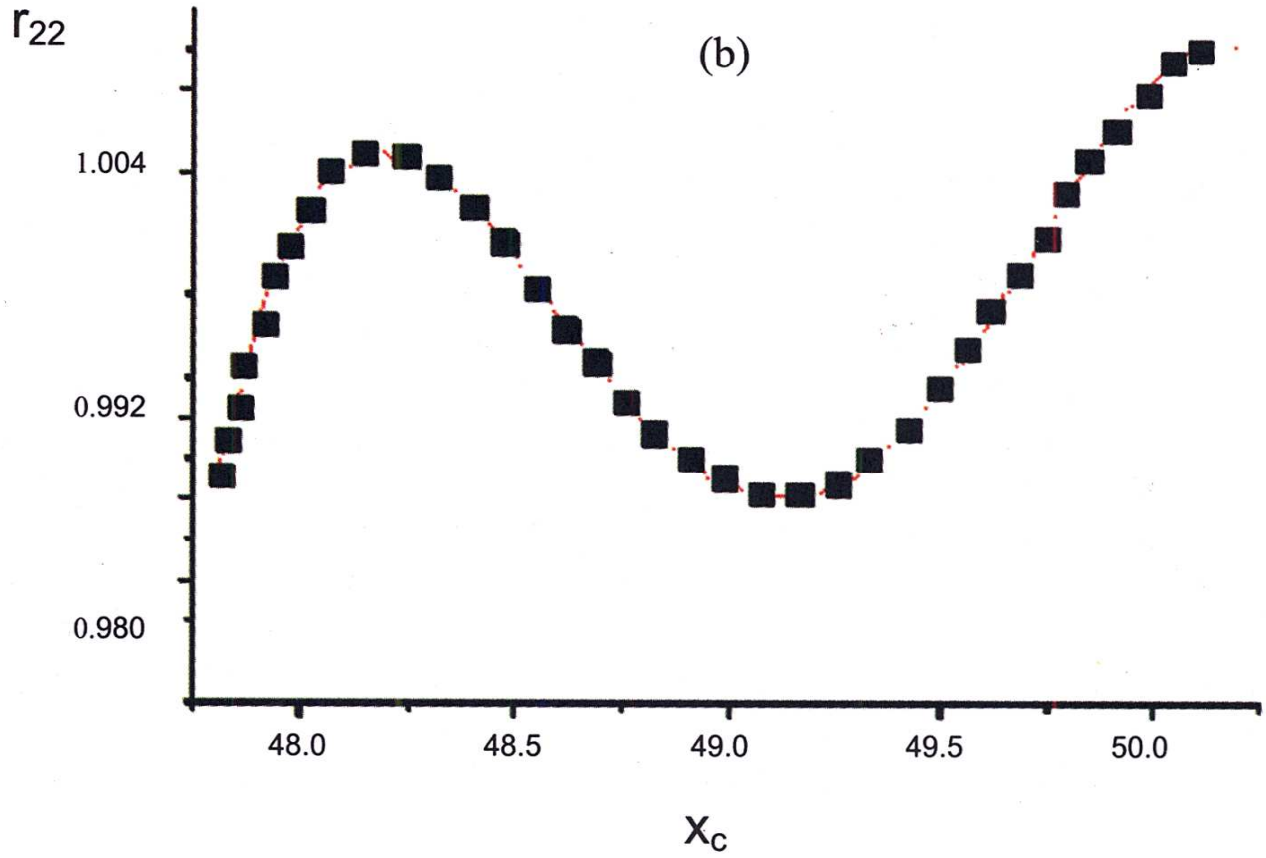

Fig. 4. Comparison between the calculated (a) and experimental (b) behaviours in the crystal composition dependence of the EO coefficient r_{22}

Conclusions

The proposed in the present work *ab initio* band energy approach with the molecular dynamics geometry optimisation procedure seems to be sufficient for explaining of the main features in the non-stoichiometry-spectral-dependent behaviours of the electrooptic coefficients. An appearance of the depth in the electrooptic coefficients is caused by a competition between the long-range order 2pO-2sLi band contributions disturbed by the oxygen vacancies and by the localised 3dNb-2pO cluster fragments. Molecular dynamics methods unambiguously show an occurrence of a correlation between the band states behaviours (optical oscillators at 4.8 and 6.82 eV) and non-centrosymmetry of electrostatic potential for the particular [Nb-O_6] clusters. Inclusion of the phonon subsystem shifts a non-stoichiometry minimum very close to the experimental one. However several discrepancy remains for the value of the particular depth. In our opinion this problem can be resolved in future by inclusion of the intercluster fragments and taking into account of the higher order anharmonic interactions and new cluster configurations in order to determine the absolute values of the electrooptics coefficients r_{22}. An essential influence of near-the-defect oxygen on the non-centrosymmetry of the electrostatic potential is shown. Electronic part of the [Nb-O] clusters gives more than 50% to the total output electro-optic coefficient r_{22}. The phonon subsystem essentially increases its contribution to r_{22} within the X_c = 48.4 – – 48.8 % causing several disturbances of the long-range translations.

References

[1] U. Schlarb, K. Betzler, Phys. Rev. **B 48** (1993) 15613.

[2] F. Abdi, M. Aillerie, P. Bourson, M.D. Fontana, K. Polgar, J.Appl.Phys. **84**, (1998) 2251.

[3] M. Wohleke, G. Corradi, K. Betzler, Appl.Phys., **B 63** (1996) 323.

[4] L. Kovacs, G. Ruschhaupt, K. Polgar, C. Corradi, M. Wohleke, Appl.Phys.Lett., **70** (1997) 2801.

[5] A. Ridah, P. Bourson, M.D. Fontana, G. Malovichko, J. Phys.: Cond. Matt. **9**, (1997) 9697.

[6] H. Donnerberg, Atomic Simulation of Electrooptic and Magnetooptic oxide materials, Univ.Osnaabruck, Springer-Verlag, 1999, Berlin 33.

[7] I.V. Kityk, B. Sahraoui, Phys.Rev., **B 60** (1999) 494.

[8] E.H. Turner, F.R. Nash, P.M. Bridenbouigh, J.Appl.Phys., **42** (1971) 4155.

[9] M. Malachowski, I.R. Kityk, B. Sahraoui, Phys. Status Solidi **207,** (1998) 405.

[10] I.V. Kityk, I.N. Yaszczishin, L.V. Tyagnyriadko, Glass Physics Chemistry **20** (1994) 404.

[11] E. Golis, I.V. Kityk, J. Kasperczyk, J. Wasylak, Materials Research Bulletin **9** (1996) 1057.

[12] G.B. Bachelet, D.R. Hamann, M.Schluter, Phys. Rev. B **26** (1982) 4199.

[13] M.I. Kolinko, Phys. Rev., **B 55** (1997) 5007.

[14] I.V. Kityk, Phys.Solid State **33** (1991) 1026.

[15] I.V. Kityk, and E. Jakubczyk, Applied Optics, **38** (1999) 5162.

[16] I.V. Kityk, B. Sahraoui, P.X. Nguyen, G. Rivoire, J. Kasperczyk, Nonlinear Optics **18** (1997) 13.

[17] J.B. Perdew, A. Zunger, Phys. Rev., B **23** (1981) 5048.

[18] D.M. Ceperley, B.J. Adler, Phys. Rev.Letters **45** (1980) 161.

[19] D.J. Chadhi, M.L. Cohen, Phys. Rev. B **8** (1973) 5747.

[20] W.-Y. Ching, Z.-Q. Gu, Y.-N. Xu, Phys. Rev., B **50** (1994) 1992.

[21] I.V. Kityk, Ukr.Phys. J., **32** (1990) 678.

[22] A.D.Becke, J.Chem.Phys **98**, (1994) 1372 and 5648.

[23] Gamess, Package of the computer programms, 1997, 235 p.

I.V. KITYK, M. MAKOWSKA-JANUSIK, J. BERDOWSKI
M.D. FONTANA, M. AILLERIE AND F. ABDI

Influence of Non-stoichiometric Defects on Optical Properties in $LiNbO_3$

Summary

We present a band energy approach with a molecular dynamics cluster optimisation which accounts for the various structural modifications related to the non-stoichiometry of $LiNbO_3$ crystals. The variation of the optical properties with the deviation from the stoichiometric composition can be understood within this approach. Especial role of the electron-phonon contributions to the electrooptics coefficient is

shown. In particular, model calculations yield a large dependence of the electrooptis coefficient r_{22} on the crystal composition, in agreement with the experimental data. The observed minimum of the r_{22} coefficient versus the non-stoichiometry in the plot is interpreted as being by a diminishing in the non-centrosymmetry of the electrostatic potential around Nb-O_6 clusters.